2016 International Symposium on Nonlinear Theory and Its Applications,
NOLTA2016, Yugawara, Japan, November 27th-30th, 2016

Intrinsic Localized Modes in Saturable Inductor Transmission Lines

M. Sato†, T. Mukaide†, T. Nakaguchi†, and A. J. Sievers‡

†Graduate School of Natural Science and Technology, Kanazawa University
Kanazawa, Ishikawa 920-1192, Japan
‡Laboratory of Atomic and Solid State Physics, Cornell University
Ithaca, NY 14853-2501, USA
Email: msato153@staff.kanazawa-u.ac.jp

Abstract– Nonlinear 1-D electric transmission lines have long been used to study solitons and intrinsic localized modes (ILMs) with the focus mainly on nonlinear capacitors since they correspond to nonlinear potential energy terms in the corresponding mechanical systems. Here, we study a saturable inductor in an otherwise linear transmission line. Our simulations show ILM current waveforms strongly distorted from a sinusoidal time dependence. The well known rotating wave approximation fails to predict such an ILM; however, including the fundamental and the third harmonic of the ILM current produces results in good agreement with simulations over a restricted amplitude region.

1. Introduction

Fundamental studies focusing on a localized nonlinear excitation with width comparable to the lattice constant of a lumped nonlinear electrical transmission line have appeared in the last decade[1-4]. To date all of these intrinsic local mode (ILM) systems have made use of nonlinear capacitors to produce intersite nonlinear coupling between the linear inductor lattice sites. In the asymptotic strongly localized limit the excitation extends over three lattice cells.

In this report we describe a different kind of ILM associated with nonlinear inductors equally spaced in an otherwise linear electrical transmission line. In an earlier work, we considered a transmission line with a flux dependent inductance, where the rotating wave approximation (RWA) could be used. [5] Here a 1-D electric lattice with linear intersite capacitance coupling plus a current dependent inductance is the starting point. Our results demonstrate that an RWA that makes use of only the fundamental frequency is not sufficient to provide a realistic current ILM since strong harmonics appear in the equations of motion. Including these harmonic contributions shows that in the asymptotic strongly localized limit the excitation can extend over a single lattice cell.

2. Inductor model, circuit and equations of motion

A simple nonlinear inductor model with no hysteresis that describes saturation of the total flux Λ with respect to the current I is

$$I = \frac{1}{\sqrt{\eta}} \tan\left(\frac{\sqrt{\eta}}{L_0}\Lambda\right) \qquad (1)$$

where L_0 is the linear inductance and η is the nonlinear parameter. Figure 1 illustrates this dependence of the flux on the current. Also shown is the corresponding nonlinear inductance

$$L(I) = \frac{d\Lambda}{dI} = \frac{L_0}{1+\eta I^2} \qquad (2)$$

which decreases with increasing current.

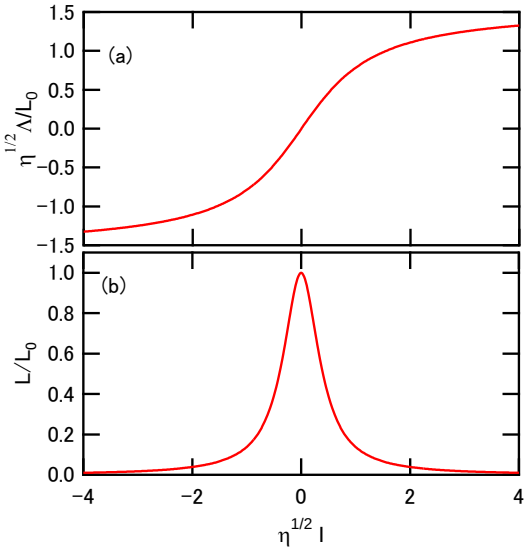

Fig. 1. (a) Current dependence of the total flux Λ through the inductor. (b) The nonlinear inductor $L(I)$ for the model describe by Eq. (1).

The transmission line under consideration is shown in Fig. 2. Because for the simulations we are interested in exciting the plane wave zone boundary mode to produce an ILM above the plane wave spectrum the transmission line is coupled to a set of drivers with opposite phase.

In the absence of the driver and the resistance the equations of motion of the current in Fig. 2 can be written as

$$\frac{1}{C}\int J_{n-1}dt = L(I_n)\frac{dI_n}{dt} + \frac{1}{C}\int J_n dt \qquad (3)$$

where the relative currents are described by $J_{n-1} = I_{n-1} - I_n$, $J_n = I_n - I_{n+1}$ and L is given by Eq. (2). Eq. (3) is readily transformed into

$$\frac{d}{dt}\left[\frac{\dot{I}_n}{1+\eta I_n^2}\right] = -\frac{\omega_m^2}{4}\left(2I_n - I_{n+1} - I_{n-1}\right) \qquad (4)$$

where $\omega_m = \sqrt{\frac{4}{L_0 C}}$ is the maximum frequency of the linear dispersion curve $2\omega^2 = \omega_m^2(1-\cos k)$. Equation (4) is similar to that for a spring-mass transmission line system with an amplitude dependent mass. The corresponding mass would become smaller with increasing amplitude.

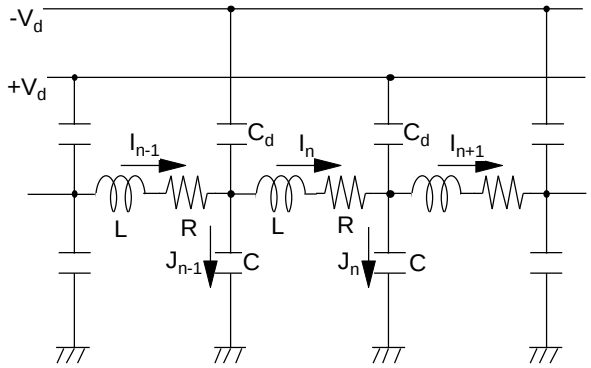

Fig. 2 Circuit diagram for a nonlinear inductor transmission line with driver lines. The transmission line is composed from the nonlinear inductors (L) and linear capacitors (C). R=inductor resistance. The transmission line is excited by a set of lines with opposite phase, via coupling capacitor C_d .

3. Driven-damped simulations

Simulations using a driven damped lattice were performed to investigate the ILM properties. Damping is caused by the resistance R in Fig. 2. The circuit is driven by an oscillator via coupling capacitors C_d as shown. Because the nonlinearity in Eq. (4) is positive, we expect the generation of an ILM to commence at the zone boundary where the normal plane wave mode frequency is largest. The equation of motion now becomes

$$\ddot{I}_n\left(1+\eta I_n^2\right) = 2\eta I_n \dot{I}_n^2$$
$$-\frac{\omega_m^2}{4}\left(2I_n - I_{n+1} - I_{n-1}\right)\left(1+2\eta I_n^2 + \eta^2 I_n^4\right), \qquad (5)$$
$$-\frac{R}{L_0}\frac{dI_n}{dt} + \frac{C_d}{L_0\left(C+C_d\right)}\left(\frac{dV_{dn-1}}{dt} - \frac{dV_{dn}}{dt}\right)$$

where last two terms are the damping and the driver, respectively.

The resulting stationary ILM is shown in Fig. 3. Figure 3(a) displays the time dependence of the ILM, and Fig. 3(b) shows its spatial pattern. The shape is appropriate for an odd symmetry mode. The driven-damped simulation of the frequency squared versus the amplitude squared is summarized by the dashed curve in Fig. 4, indicating that the mode frequency is nearly proportional to the amplitude.

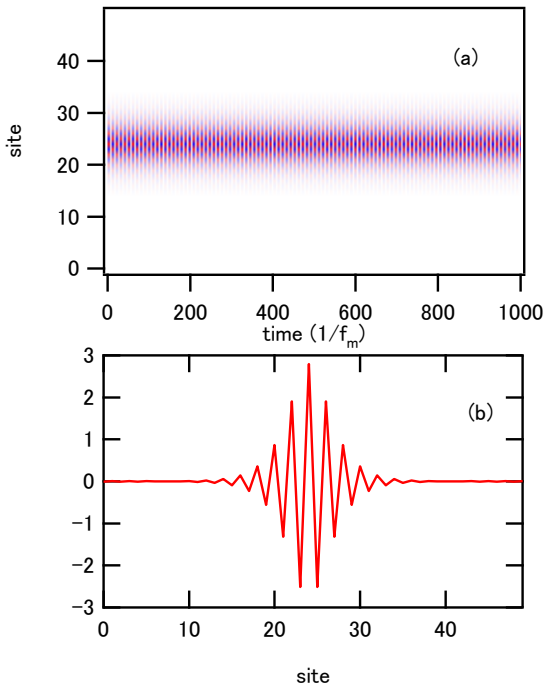

Fig. 3(a) Simulated stationary ILM at frequency $1.025 f_m$, where $f_m = \omega_m / 2\pi$. (b) Real space profile of the stationary odd symmetry ILM in panel (a).

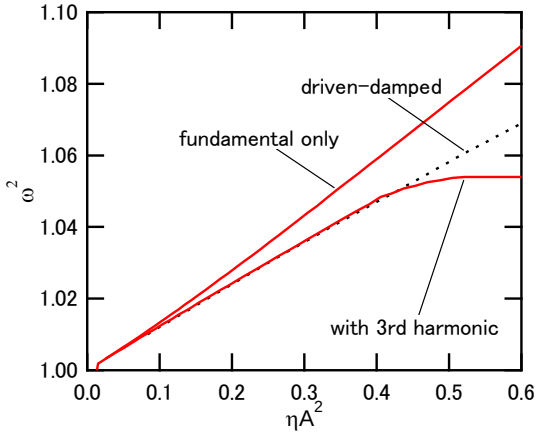

Fig. 4. Comparison of ILM simulations with a damped driver and analysis based on the RWA approximation. Square of frequency is shown as a function of ηA^2 . Analysis including the fundamental and 3rd-harmonic shows good agreement with the simulated results in the low amplitude region $\eta A^2 < 0.4$.

4. Testing the rotating wave approximation

For the first method of analysis to compare with the simulation results we used the RWA**.** We assume sinusoidal time-dependence of the current,

$$I_n = A_n \cos \omega t \quad (6)$$

and then apply the RWA to Eq. (4) to obtain the following algebraic equations

$$\begin{aligned} &-\omega^2 A_n \left(1+\frac{3}{4}\eta A^2\right) = \omega^2 \frac{1}{2}\eta A^2 A_n \\ &-\frac{\omega_m^2}{4}\left(2A_n - A_{n+1} - A_{n-1}\right)\left(1+\frac{3}{2}\eta A_n^{\,2} + \frac{5}{8}\eta^2 A_n^{\,4}\right) \end{aligned} \quad . \quad (7)$$

This set of nonlinear equations is solved using Powell's hybrid method in MINPACK software. The dependence of the ILM frequency on amplitude is represented by the highest frequency curve shown in Fig. 4. The squared frequency of the ILM increases linearly with ηA^2 but with a larger slope than does the driven-damped simulation (dashed curve).

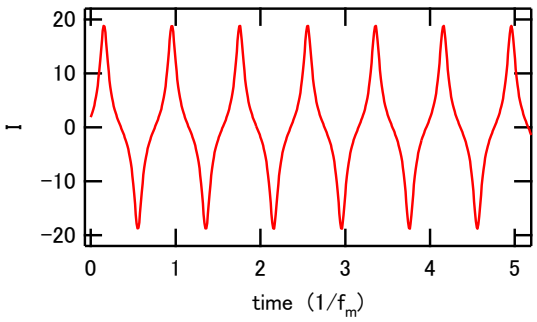

Fig. 5. Time dependence of the simulated ILM current at $1.25 f_m$. It is time periodic but distorted from a sinusoidal curve by higher harmonics.

The reason for the difference becomes obvious when one examines the time dependence of the ILM current as obtained from the driven-damped simulations. The time dependence of the current shown in Fig. 5 is very different from that given by Eq. (6).

The next step in analytic complexity is to add a third harmonic term to the ILM description. The new approximation becomes

$$I_n = A_n \cos \omega t + B_n \cos 3\omega t \quad . (8)$$

The new coefficients for the fundamental and 3rd harmonic signals are now determined from Eq. (4) in a way similar to the RWA method. The term that invalidates the RWA is the first term of right hand side of Eq. (9):

$$\ddot{I}_n\left(1+\eta I_n^2\right) = \frac{2\eta I_n \dot{I}_n^2}{1+\eta I_n^2} - \frac{\omega_m^2}{4}\left(2I_n - I_{n+1} - I_{n-1}\right)\left(1+\eta I_n^2\right). \quad (9)$$

If this term were absent, the usual RWA would work well. To proceed we expand the denominator in Eq. (9) up to 4th order in current so that

$$\begin{aligned} &\ddot{I}_n = 2\eta I_n \dot{I}_n^2\left(1-\eta I_n^2 + \eta^2 I_n^4\right) \\ &-\frac{\omega_m^2}{4}\left(2I_n - I_{n+1} - I_{n-1}\right)\left(1+\eta I_n^2\right) \end{aligned} \quad . \quad (10)$$

All terms in Eq. (10) are calculated using Eq. (8). Although tedious the calculation is straightforward. An example is given in Eq. (11).

$$\begin{aligned} &2\eta I_n \dot{I}_n^2 = \\ &\left(\frac{1}{2}A_n^3 + \frac{5}{2}A_n^2 B_n + 9A_n B_n^2\right)\omega^2 \eta \cos \omega t \\ &+\left(-\frac{1}{2}A_n^3 + A_n^2 B_n + \frac{9}{2}B_n^3\right)\omega^2 \eta \cos 3\omega t \end{aligned} \quad (11)$$

The result is $C_1 \cos \omega t + C_3 \cos 3\omega t = 0$ where C_n are total coefficient of n-th harmonic signal. By setting each coefficient equal to zero, we obtain the following algebraic equations:

$$\begin{aligned} &-\omega^2 A_n + \frac{\omega_m^2}{4}\left(2A_n - A_{n-1} - A_{n+1}\right) \\ &+\omega^2 \eta\left(-\frac{1}{2}A_n^{\,3} - \frac{5}{2}A_n^{\,2}B_n - 9A_n B_n^{\,2}\right) \\ &+\frac{3\omega_m^{\,2}}{8}\eta\left(A_n^{\,3} + A_n^{\,2}B_n + 2A_n B_n^{\,2}\right) \\ &-\frac{\omega_m^2}{16}\eta\left(\begin{array}{l}\left(3A_n^{\,2} + 2A_n B_n + 2B_n^{\,2}\right)\left(A_{n+1} + A_{n-1}\right) \\ +\left(A_n^{\,2} + 4A_n B_n\right)\left(B_{n+1} + B_{n-1}\right)\end{array}\right) \\ &+\frac{1}{8}\eta^2\omega^2\left(\begin{array}{l}2A_n^{\,5} + 15A_n^{\,4}B_n + 60A_n^{\,3}B_n^{\,2} \\ +42A_n^{\,2}B_n^{\,3} + 54A_n B_n^{\,4}\end{array}\right) \\ &-\frac{1}{32}\eta^3\omega^2\left(\begin{array}{l}5A_n^{\,7} + 49A_n^{\,6}B_n + 231A_n^{\,5}B_n^{\,2} + 375A_n^{\,4}B_n^3 \\ +570A_n^{\,3}B_n^{\,4} + 230A_n^{\,2}B_n^{\,5} + 180A_n B_n^{\,6}\end{array}\right) \\ &= 0 \end{aligned} \quad (12)$$

and

$$
\begin{aligned}
&-9\omega^2 B_n + \frac{\omega_m^2}{4}\left(2B_n - B_{n-1} - B_{n+1}\right) \\
&+\omega^2\eta\left(\frac{1}{2}A_n{}^3 - A_n{}^2 B_n - \frac{9}{2}B_n{}^3\right) \\
&+\frac{\omega_m{}^2}{8}\eta\left(A_n{}^3 + 6A_n{}^2 B_n + 3B_n{}^3\right) \\
&-\frac{\omega_m^2}{16}\eta\begin{pmatrix}\left(A_n{}^2 + 4A_n B_n\right)\left(A_{n+1} + A_{n-1}\right) \\ +\left(2A_n{}^2 + 3B_n{}^2\right)\left(B_{n+1} + B_{n-1}\right)\end{pmatrix} \\
&+\frac{1}{8}\eta^2\omega^2\begin{pmatrix}A_n{}^5 + 6A_n{}^4 B_n + 18A_n{}^3 B_n{}^2 \\ +60A_n{}^2 B_n{}^3 + 18B_n{}^5\end{pmatrix} \\
&-\frac{1}{32}\eta^3\omega^2\begin{pmatrix}-A_n{}^7 + 21A_n{}^6 B_n + 105A_n{}^5 B_n{}^2 + 330A_n^4 B_n^3 \\ +250A_n{}^3 B_n{}^4 + 380A_n{}^2 B_n{}^5 + 45B_n{}^7\end{pmatrix} \\
&= 0
\end{aligned}
\qquad .(13)
$$

Solving the two set of equations for N lattice points, we obtain the squared frequency as a function of ηA^2 as shown by the lowest frequency trace in Fig. 4. Good agreement with the simulations does occur but only below $\eta A^2 < 0.4$.

5. Discussion and Summary

The source of the periodic sharp peaking of the ILM current with time is the nonlinear inductance. That is, the inductance becomes the smallest at the current peak. Although the slope of the current is zero at the peak, it changes more rapidly near the peak than for the constant inductance case and this feature produces the narrowing of the current peak shown in Fig. 5.

Above an amplitude of $\eta A^2 > 0.4$, the rate of change of the inductance becomes larger as shown in Fig. 1(b). This property introduces higher harmonics than used in Eq. (7). For this reason, our second attempt at an analytical determination of the ILM properties failed for large amplitudes. Thus the general features of an ILM associated with current saturable inductors in a 1D transmission line are threefold: (1) the RWA can not be applied to obtain an analytical solution, (2) in the asymptotic limit the ILM excitation becomes localized on a single lattice cell and (3) this ILM contains many harmonics of the fundamental ILM frequency.

Acknowledgement

M. S. was supported by JSPS-Grant-in-Aid for Scientific Research No. 25400394. A. J. S. acknowledges the hospitality of the Department of Physics and Astronomy, University of Denver, where some of this work was completed.

References

[1] M. Sato, S. Yasui, M. Kimura, T. Hikihara, and A. J. Sievers, Europhys. Lett. **80**, 30002 (2007).

[2] L. Q. English, R. B. Thakur, and R. Stearrett, Phys. Rev. E **77**, 066601 (2008).

[3] L. Q. English, F. Palmero, A. J. Sievers, P. G. Kevrekidis, and D. H. Barnak, Phys. Rev. E **81**, 046605 (2010).

[4] L. Q. English, F. Palmero, J. F. Stormes, J. Cuevas, R. Carretero-González, and P. G. Kevrekidis, Phys. Rev. E **88**, 022912 (2013).

[5] M. Sato, T. Mukaide, T. Nakaguchi, and A. J. Sievers, arXiv:1607.03962, Phys. Rev. E **94,** 012223(2016).